Data-based fractional differential models for non-linear dynamic modeling of a lithium-ion battery

Yunfeng Jiang [a, *], Bing Xia [b, c], Xin Zhao [a], Truong Nguyen [c], Chris Mi [b], Raymond A. de Callafon [a]

[a] Department of Mechanical and Aerospace Engineering, University of California San Diego, 9500 Gilman Drive, La Jolla, CA 92093, USA
[b] Department of Electrical and Computer Engineering, San Diego State University, 5500 Campanile Drive, San Diego, CA 92182, USA
[c] Department of Electrical and Computer Engineering, University of California San Diego, 9500 Gilman Drive, La Jolla, CA 92093, USA

A B S T R A C T

This paper presents a battery model with non-integer order derivatives for modeling the dynamics of a lithium-ion battery over a large operating range. The non-integer or fractional differential model includes a constant phase element term to approximate the non-linear dynamical behavior of the battery. The proposed fractional differential model is an amalgamation of electrochemical impedance spectroscopy experimental data and standard 1-resistor-capacitor electrical circuit model. The standard least squares-based state-variable filter identification method used for continuous-time system identification is used to estimate the model parameters and the fractional derivative coefficients of the proposed fractional differential model. For application of modeling fractional differential order battery dynamics, the continuous-time least squares-based state-variable filter parameter estimation approach is extended to an instrumental variable method to be robust to (non-white) noise perturbed output measurement. The model accuracy and model performance are validated on experimental data obtained from a lithium-ion battery and confirm that the proposed fractional differential model is able to accurately capture the battery dynamics over broad operating range. In comparison, the fractional differential model shows significant improvement on data prediction accuracy compared to a conventional integer model, making the fractional differential model suitable for monitoring battery dynamical behavior in a battery management system.

© 2017 Elsevier Ltd. All rights reserved.

1. Introduction

Rechargeable batteries have currently been developed to power an ever-increasing diverse range of electrical applications in automobile starters, portable consumer devices, light vehicles, uninterruptible power supplies, and battery storage power stations [1]. State-of-the-art lithium-ion (Li-ion) batteries are considered as one of the most popular types of rechargeable batteries, exhibiting significant improvements in energy density, offering weight, size and design flexibility, appearing a very slow loss-of-charge when not in use and exhibiting negligible memory effect [2]. Beyond all these dominant features, low investment and maintenance costs drive Li-ion batteries to grow as the predominant technology for next promising generation distributed energy storage systems

(DESS) in automotive industry [3].

In the automotive sector, Li-ion batteries are becoming a common replacement for existing lead-acid and nickel-metal hydride batteries (NiMH) that have been widely applied in electric vehicles (EVs), hybrid electric vehicles (HEVs), and plug-in hybrid electric vehicle (PHEVs) [4]. Unfortunately, this replacement is a challenging task, since overheating or overcharging does cause undesirable and irreversible damage to the battery. The irreversible damages manifest itself as a degraded cell storage capacity and reduces the useful lifetime of the battery [5].

To protect the battery, a battery management system (BMS) is used to track a rechargeable battery (cell or battery pack) by monitoring the state of the battery, protecting the battery from operating outside a safe operating area and maintaining safe, reliable and optimal operation [6]. One of the most important functions of a BMS is the software use to execute algorithms that accurately capture the battery dynamics, and continuously estimate

non-measurable states, such as: state of charge (SOC), state of health (SOH) and state of power (SOP) of the battery [7].

A specific example of BMS in EV application is shown in Fig. 1, where current (I), voltage (V), power (P) and possibly battery temperature (T) are compared and predicted based on an internal model to allow for system monitoring and battery fault detection [8]. Among all above mentioned functionalities of the BMS, the primary task of all BMS features is to monitor the state of the battery (measurable/non-measurable). This is especially important to track physical parameters that may change over time as the battery cell ages and the number of total cycle increases [9].

A battery model can be described by a physics-based electrochemical model that uses a set of partial differential equations (PDEs). A typical physics-based electrochemical PDE model uses an insertion composite cathode, a solid polymer electrolyte, and a lithium anode to account for battery dynamics underlying electrochemistry principles. Such a physics-based model has the advantage of being able to describe specific battery information in terms of various physical processes occurring inside a battery. Unfortunately, it suffers from the disadvantage of model uncertainty for which parameter estimation techniques may be used. Moreover, the complexity of a physics-based model may suffer from parameter identifiability limitations, especially when only the external information of voltage, current and temperature, is available [10].

To simplify parameter estimation and simulation calculations, model complexity reduction can be considered via porous electrode models that use a single particle model (SPM) or a polynomial approximation model (PAM). A parabolic profile is utilized to approximate the concentration within each spherical particle of both electrodes in a PAM. Similarly, a single spherical particle, where area is equal to the active area of the solid phase in the porous electrode, is applied to represent each electrode in a SPM [11]. Although both simplified PAM and SPM are computationally much faster than standard physics-based models, they still have own limitations to estimate battery performance, because simplified models do not consider all physics processes [12].

Due to relatively simple structure, equivalent circuit models (ECM) are widely gaining popularity as another alternative model in designing a model for the BMS. An ECM has far less model parameters (to be estimated) and the underlying ordinary differential equation model simplifies firmware implementation. A resistor-capacitor (RC) network model, consisting of internal resistance, effective capacitance and equivalent potential, is widely applied in constructing ECM models to mimic the phenomenological effects of a battery [13]. There are some commonly applied RC network models, such as 1-RC model, 2-RC model and 1-RC hysteresis model. Although RC network models have clear electrical interpretations, the internal model properties that include the finite integer order and linearity, are not able to capture the partial derivative nature of a Li-ion battery over the full operating range. The limitations of RC network models can be observed particularly well when comparing the structural mismatch of experimental measurements of characterizing electrochemical systems [14].

One of the measurements that characterizes the dynamics of a battery system is the electrochemical impedance spectroscopy (EIS) technique. The EIS uses data obtained by excitation with a small voltage and experimentally measures the impedance of the system as a function of frequency. The frequency response of the measured system obtained by EIS measured data is revealed to express energy storage, battery internal states, and dissipation properties in a Nyquist plot. As an illustration in Fig. 2, there are two main sections in the typical Nyquist plot of a Li-ion battery over full operating frequency range: (1) a low frequency range (1 mHz-1 Hz)
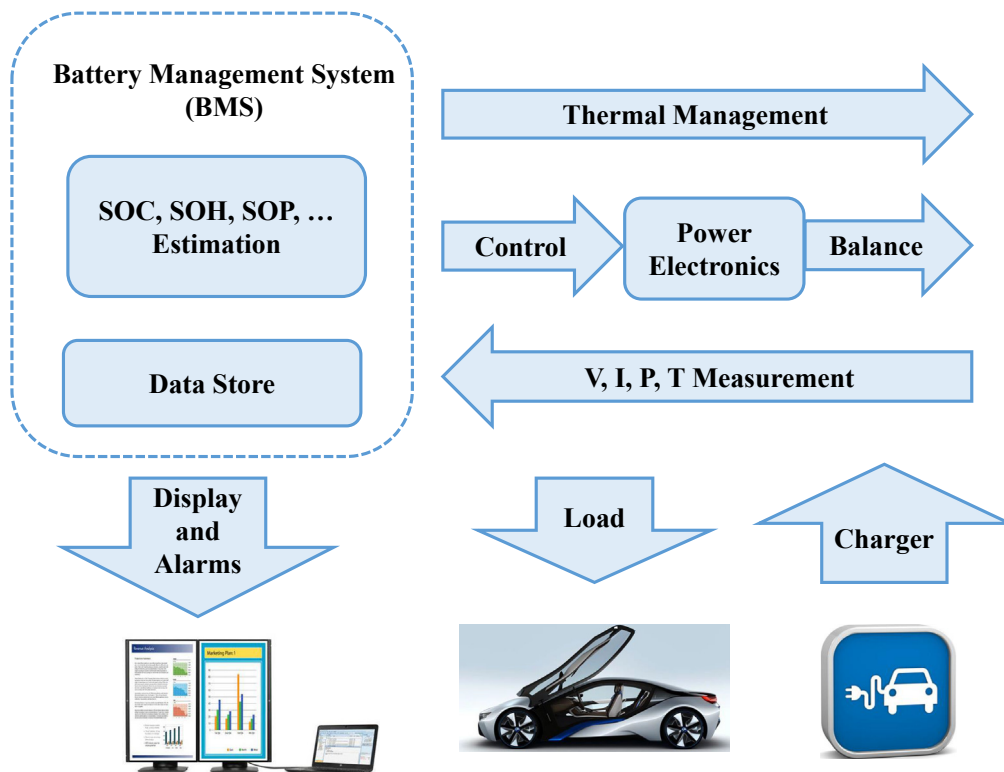

Fig. 1. Overall architecture of a specific example of battery management system (BMS) in electric vehicle (EV) application.
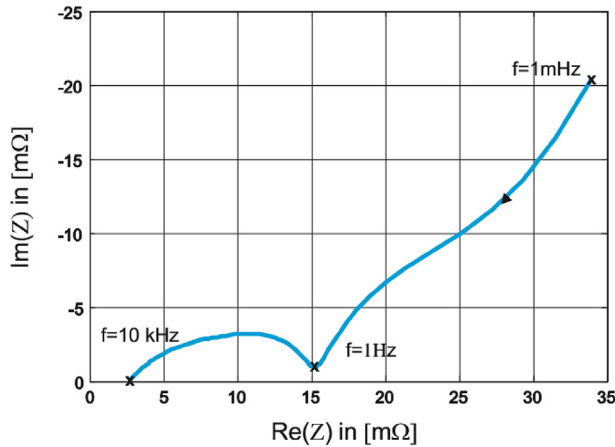
Fig. 2. Typical Nyquist plot of a Li-ion battery cell [17].

where a straight line characterized by the 45° is usually believed to be caused by limitations in mass diffusion of lithium ions; (2) a middle frequency range (1 Hz- 10 kHz), where a semi-ellipse can be attributed to the charge transfer process, porosity of the electrodes, and double-layer effect to represent the kinetics of the electrochemical battery reactions [15]. The most simple 1-RC network ECM shows an ideal semi-circle in the EIS graph, which is not consistent with measured experimental data displayed in Fig. 2. Although increasing the model order by adding more RC components may be used to improve the data fit, it suffers from a large number of model parameters to be estimated. Therefore, it is necessary to figure out a simple model to accurately capture the non-linear behavior over the full operating range of typical Li-ion battery Nyquist plot, motivated by structure mismatch and complicated parameter estimation of integer ECMs.

An alternative and successful approach to find accurate, but still low complexity models of battery systems is to use a fractional differential model (FDM). A FDM has non-integer derivatives for states can be applied to fix reconcile discrepancies between structure complexity and estimation accuracy in common ECMs. FDMs are able to explain inherent fractional derivative properties due to diffusion dynamics, memory hysteresis, and mass transfer of Li-ion batteries, thus they have ability to exhibit better accuracy with fewer parameters, compared with conventional integer ECMs [16].

There are various parameter identification approaches that can be employed to determine the unknown parameters of a FDM for a battery system. A recently published parameter estimation method [17] has shown to provide good results, but requires a large number of time consuming integration and convolution calculations. In addition, this method requires noise-sensitive identification to estimate the fractional derivative value. Although alternate indirect identification method of discrete-time (DT) model parameters can be used to solve the above issues, information on fast dynamics may be lost due to sampling, whereas relatively too small sampling time will result to numerical problems that limits DT model identification [18]. Furthermore, estimation of model parameters may be sensitive to initial and noise conditions and limits the potential of real-time applications [19]. In order to overcome disadvantages of DT method, a direct CT system identification can been applied, because it can provide good insight of system properties and avoid information loss due to undesired high sensitivity issues [20]. Compared with conventional least squares (LS) identification methods, instrumental variable (IV) methods have the advantages of providing consistent parameter estimates when the noise in real

applications can not comply with a normal distribution and rational spectral density [21]. As one of the available IV methods, the simplified refined instrumental variable for continuous-time system identification (SRIVC), is able to exhibit statistically consistent and asymptotically efficient parameter estimates in the presence of white measurement noise [22]. The main reason of selecting instrumental variable state-variable filter (IVSVF) method is because of its ability to provide consistent estimate results for non-white noise structure in Li-ion experimental measurement cases [23].

Based on the premise of using the advantage of CT identification for the estimation of model parameters, the main purposes of this paper is to show the following contributions: (1) a FDM that has fewer estimation parameters than a physics-based electrochemical model, can be applied to accurately mimic complex input/output dynamic behavior of an electrochemistry-based system inside a Li-ion battery; (2) a CT system identification approach can be used to estimate model parameters of a FDM in a Li-ion battery; (3) the use of a state-variable filter (SVF) to formulate a parameter estimation problem that is less susceptible to noise on the fractional derivatives of the input/output signals of the model; (4) the use of a standard least squares based state-variable filter (LSSVF) method for the estimation of FDM parameters; (5) the further improvement of the LS parameter estimates via an instrumental variable (IV) method to estimate parameters of the FDM.

2. Fractional differential systems

Fractional differential systems have been widely applied in various application fields, such as physical chemistry, electricity, electronics, mechanics, automatic control, robotics and signal processing, because their dynamics behaviors can be described by differential equations involving fractional derivatives functions (fractional differential equations) [24]. For most dielectric/insulating materials in electrical application, the current and the voltage across the capacitor are non-linear related: the current is proportional to time non-integer derivative of the voltage across the capacitor [25]. Also, unlike the well-known conventional "integer" methods, the non-integer derivative allows an explanation of mass transport, diffusion, and memory in dielectrics [26]. For a battery system, especially Li-ion battery system, the fractional differential system is applied in capturing the electrical dynamics including mass transport and charge transfer process in the electrolyte, mass diffusion and porosity in solid electrodes [27].

2.1. General linear fractional differential system equation

A general linear fractional differential system can be expressed by a fractional differential equation of the following form

$$y(t) + a_1 D^{\alpha_1} y(t) + \ldots + a_n D^{\alpha_n} y(t)$$
$$= b_0 D^{\beta_0} u(t) + b_1 D^{\beta_1} u(t) + \ldots + b_m D^{\beta_m} u(t) \tag{1}$$

where $(a_j, b_i) \in \mathbb{R}^2$, differentiation orders $\alpha_1 < \alpha_2 < \ldots < \alpha_n$, $\beta_0 < \beta_1 < \ldots < \beta_m$, and $\alpha_i, \beta_i \in \mathbb{R}^+$ (restricted to arbitrary positive real-number value). The fractional differentiation operator for real-number value of α when α takes a non-integer value can be defined as [28]

$$D^{\alpha} = \left(\frac{d}{dt}\right)^{\alpha}, \quad \forall \alpha \in \mathbb{R}^+ \tag{2}$$

The classical form of fractional derivative in Riemann-Liouville (R-L) sense to a function $f(t)$ is commonly defined by Ref. [25]

$$D^\alpha f(t) = \left(\frac{d}{dt}\right)^{\lceil\alpha\rceil} \frac{1}{\Gamma(\lceil\alpha\rceil - \alpha)} \int_0^t \frac{f(\tau)}{(t-\tau)^{\alpha-\lceil\alpha\rceil}} d\tau \qquad (3)$$

where $\forall \alpha \in \mathbb{R}^+$, $t > 0$, and gamma function $\Gamma(\gamma)$ for every $\gamma \in \mathbb{R}^+$ can be defined via a convergent improper integral:

$$\Gamma(\gamma) = \int_0^\infty z^{\gamma-1} e^{-z} dz \qquad (4)$$

It should be noted that in the above equations the floor function $\lfloor\cdot\rfloor$ represents the largest integer smaller than or equal to α, and the ceiling function $\lceil\cdot\rceil$ defines the smallest integer larger than or equal to α. An alternative definition called Grünwald-Letnikov (G-L) allows the derivative a non-integer value instead of the integral is considered as the following definition [26]

$$D^\alpha f(t) = \lim_{h \to 0} \frac{(-1)^\alpha}{h^\alpha} \sum_{j=0}^{\left[\frac{t-a}{h}\right]} (-1)^j \binom{\alpha}{j} f(t+jh) \qquad (5)$$

where $[\cdot]$ donates the integer part. The Laplace transform of α-th derivative ($\alpha \in \mathbb{R}^+$) of an arbitrary signal $f(t)$

$$\mathscr{L}\{D^\alpha f(t)\} = s^\alpha F(s), \text{ if } f(t) = 0 \; \forall t \leq 0 \qquad (6)$$

can then be generally applied as a more concise algebraic tool to describe fractional differential systems [29]. Thus this allows to rewrite the fractional differential equation (1), with both input signal $u(t)$ and output signal $y(t)$ equal to 0 when $t = 0$ (zero initial conditions), into a transfer function form

$$G(s) = \frac{b_0 s^{\beta_0} + b_1 s^{\beta_1} + \cdots + b_m s^{\beta_m}}{1 + a_1 s^{\alpha_1} + \cdots + a_n s^{\alpha_n}} \qquad (7)$$

The transfer function $G(s)$ in (7) is applied in the continuous-time identification of the FDMs throughout this paper.

2.2. Numerical analysis of fractional derivatives

The reversed Grünwald-Letnikov (reversed G-L) definition in the similar form with (5)

$$D^\alpha f(t) = \lim_{h \to 0} \frac{1}{h^\alpha} \sum_{j=0}^{\left[\frac{t-a}{h}\right]} (-1)^j \binom{\alpha}{j} f(t-jh) \qquad (8)$$

is carried out to simulate the system response to an arbitrary input signal in time-domain analysis of a fractional derivative system. The closed-form numerical solution to the general fractional differential equation (1) in reversed G-L form can be computed by the recursive approach [30]

$$y_t = \frac{1}{\sum_{i=0}^n \frac{a_i}{h^{\alpha_i}}} \left(u_t - \sum_{i=0}^n \frac{a_i}{h^{\alpha_i}} \sum_{j=1}^{\left[\frac{t-a}{h}\right]} w_j^{(\alpha_j)} y_{t-jh} \right) \qquad (9)$$

where h represents the step-size in computation. The $w_j(\alpha)$ in the above solution (9) can be evaluated recursively from

$$w_0^\alpha = 1, w_j^\alpha = \left(1 - \frac{\alpha+1}{j}\right) w_{j-1}^\alpha, j = 1, 2, \ldots \qquad (10)$$

The above recursive method can be applied to obtain numerical approximation of fractional derivative input and output signals. The signal $\hat{u}(t)$ is calculated by using (8) substituting $(-1)^\alpha \binom{\alpha}{j} = w_j^\alpha$ and the time response under the signal $u(t)$ can be consequently obtained. Since the recursive approach is based on the fixed-step computation, the step-size h needs to be selected with special care to improve the accuracy of the simulation. Therefore, it is necessary to take sometime to validate the computational results by decreasing step-size h in a gradual way until the simulation results have no variation.

3. Continuous-time system identification

The direct continuous-time (CT) system identification has been analyzed and compared with indirect discrete-time (DT) system identification methods in battery applications [31].

3.1. Advantages of continuous-time over discrete-time model identification

DT model identification based on sampled input/output data set has been successfully applied in estimation of CT dynamics processes by digital computers and data acquisition systems (DAS). However, the difficulties or limitations of using DT model identification in Li-ion battery applications have been encountered when applying various sampling rate (or sampling interval). High sampling rate can lead to numerical problems due to discrete poles constrained in small area close to the unit circle boundary of the z-plane, whereas low sampling rate is not able to retain all the system information [32]. Since Li-ion battery system consists of both fast and slow dynamic modes of behavior, which reveals a typical stiff system, the selection of sampling rate (sampling interval) needs to be treated with excessive care [33]. On the one hand, the slow sampling (large sampling interval) will lead to the information loss due to the existence of the fast dynamics. On the other hand, the rapid sampling (small sampling interval) is able to accurately capture the fast system dynamic, however, this will result in the inaccuracy of parameter estimation because of ignorance of the slow dynamics in real system [34]. Moreover, the numerical precision of DT system is more inclined to be affected by the estimation parameters and the discrete pole location that is located near the stability boundary within limited storage resolution [35]. As the sampling rate increases, the disturbance sensitivity of capacitance and resistance values increases the quasilinear utility in the RC networks, which ultimately leads to inaccurate results of the system identification [36].

The direct CT system identification has been thoroughly studied in contrast with the indirect DT identification [37]. When applied to model identification and parameter estimation in using data collected when choosing the appropriate sampling rate, the CT identification methods have particular advantages over well-established DT methods for system modeling and control system design: (1) the CT identification methods are preferable to represent underlying dynamic system in better physical insight, exhibit the preservation of a priori knowledge, and show built-in capability to deal with the situation of non-uniformly sampled data; (2) the CT approach includes inherent filtering, which not only can significantly improve the statistical efficiency, but also makes more robust to measurement noises; (3) the CT identification method can efficiently avoid discretization that induces undesired high

sensitivity issues, therefore it can result in better identification performance of the stiff system [38]. Therefore, considered all above advantages, the direct CT identification approach is utilized to the parameter identification throughout the paper.

3.2. Conventional least squares-based state-variable filter method

In order to consider CT parameter estimation of the FDM in (1) or transfer function $G(s)$ in (7), it is assumed that measurable output signal $y(t)$ is corrupted by an additive measurement white noise $e(t)$

$$y(t) = y_0(t) + e(t) \tag{11}$$

where $y_0(t)$ is hypothetical noise-free deterministic system output. It is worth noting that the input signal $u(t)$ and the output signal $y(t)$ are considered to be related with the fractional differential equation (1). Therefore, the equation error is then expressed as the following form [39]

$$\varepsilon(t) = y(t) - \varphi(t)^T \theta \tag{12}$$

where the regressor vector is defined as

$$\varphi(t) = \left[D^{\beta_0} u(t) \ \dots \ D^{\beta_m} u(t) \ -D^{\alpha_1} y(t) \ \dots \ -D^{\alpha_n} y(t) \right]^T \tag{13}$$

and the parameter is denoted by the vector

$$\theta = [b_0 \ b_1 \ \dots \ b_m \ a_1 \ a_2 \ \dots \ a_n]^T \tag{14}$$

A mathematical approach to determine parameter vector θ is minimizing L_2 norm of $\varepsilon(t)$

$$J = \int_0^T (\varepsilon(t))^2 dt \tag{15}$$

In the present case, output signal $y(t)$ is highly linear to the parameter vector θ, thus J is minimized analytically in the following least squares (LS) estimate

$$\widehat{\theta}_{LS} = \left(\int_0^T \varphi(t)^T \varphi(t) dt \right)^{-1} \int_0^T \varphi(t)^T y(t) dt \tag{16}$$

In order to numerically compute the LS estimate in (16), the discretization of fractional derivative input and output signals is needed to transfer continuous functions and equations into discrete counterparts. Considering time digitized regression vector $\varphi(kT_s)$, time instant T_s and $k = 1, 2, \dots, N$ based on N data points, the regressor matrix $\mathbf{\Phi}$ can be then formulated as

$$\mathbf{\Phi} = [\varphi(T_s) \ \varphi(2T_s) \ \dots \ \varphi(NT_s)]^T \tag{17}$$

and the digitized system output $y(kT_s)$ can be formed as a column vector to describe output matrix $\mathbf{Y}$ in a similar way. The CT LS parameter estimation can be computed via

$$\widehat{\theta}_{LS} = \left(\mathbf{\Phi}^T \mathbf{\Phi} \right)^{-1} \mathbf{\Phi}^T \mathbf{Y} \tag{18}$$

Because CT stochastic processes are always related with the white noise and its derivatives, parameter estimation normally would encounter difficulties: small perturbations that contaminating on the coefficient or the initial condition of the differential equation would finally result in the perturbations of the solution

[40]. Therefore, special care is needed in parameter estimation of the fully stochastic FDM CT model in order to reduce the noise/deviation on the input/output data in order to alleviate the practical difficulties. A traditional and effective approach to estimate coefficients of (fractional order) CT model is to use a minimum-order SVF filter to both sides of (12) [41]. From the signal analysis perspective, the SVF consisted of multiple band-pass filters can be applied to gain differentiation behavior in low frequency part, and to filter (smooth) noise/perturbation effect in high frequency part. A typical SVF filter is chosen with operator model $L(s)$ in the following form [42]

$$L(s) = \frac{1}{E(s)} = \left(\frac{\gamma}{s + \gamma} \right)^n \tag{19}$$

where n is the highest system order, and γ represents the cut-off frequency of the SVF. It should be noted that since the cut-off frequency γ is selected to emphasize the filter frequency band and define the bandwidth of the filter, the recommended γ value in general is chosen to be slightly larger than the frequency bandwidth of the identified system [32]. Hence, filtered input u_f and output y_f can be obtained at the output of the filters (19)

$$u_f(t) = L(s)u(t) \tag{20}$$

and

$$y_f(t) = L(s)y(t) \tag{21}$$

By using the filters defined in (19), the fractional equation (1) can be extended to the (fractional) derivatives form as to formulate the standard least squares-based SVF (LSSVF) method

$$y_f(t) + a_1 D^{\alpha_1} y_f(t) + \dots + a_n D^{\alpha_n} y_f(t)$$
$$= b_0 D^{\beta_0} u_f(t) + b_1 D^{\beta_1} u_f(t) + \dots + b_m D^{\beta_m} u_f(t) \tag{22}$$

Instead of minimizing the L_2 norm of $\varepsilon(t)$ as in (12), the L_2 norm of $\varepsilon_f(t)$ is now minimized based on the filtered fractional equation in (22)

$$\varepsilon_f(t) = y_f(t) - \varphi_f(t)^T \theta \tag{23}$$

where the regressor vector is composed of the filtered input/output signals as the following form

$$\varphi_f(t) = \left[D^{\beta_0} u_f(t) \ \dots \ D^{\beta_m} u_f(t) \ -D^{\alpha_1} y_f(t) \ \dots \ -D^{\alpha_n} y_f(t) \right]^T \tag{24}$$

Again, the same discretization approach is applied to numerically compute the (fractional) derivatives of the input/output signals to estimate parameters. Combined a time digitized filtered regression vector $\varphi_f(kT_s)$ with the filtered system output $y_f(kT_s)$ column vector $\mathbf{Y}_f$, time instant T_s and $k = 1, 2, \dots, N$, the CT LSSVF estimate can be formulated as

$$\widehat{\theta}_{LSSVF} = \left(\mathbf{\Phi}_f^T \mathbf{\Phi}_f \right)^{-1} \mathbf{\Phi}_f^T \mathbf{Y}_f \tag{25}$$

where

$$\mathbf{\Phi}_f = \left[\varphi_f(T_s) \ \varphi_f(2T_s) \ \dots \ \varphi_f(NT_s) \right]^T \tag{26}$$

3.3. Instrumental variable-based state-variable filter method

The basic LSSVF method has some attractive properties and include the analytical solution that is relatively easy to compute, low computational complexity, and quite good robustness with respect to noise. However, it is well known the resultant parameter estimates are asymptotically biased in the presence of non-white equation noise on the regression equation. The main reason comes from the fact that the filtered regression vector $\varphi_f(kT_s)$ is correlated with the filtered noise term $\varepsilon_f(kT_s)$ [37]. As a traditional variant of the LS method, the instrumental variable (IV) method can deliver unbiased estimates and also has the advantage of relying on linear regression techniques.

The primary principle of the IV method relies on the so-called instruments generally obtained from a parallel model y_f^{IV}. Hence, the most common IV identification method uses an auxiliary model in order to generate noise-free output estimate

$$\varphi_f^{IV}(t) = \left[D^{\beta_0} u_f(t) \ \dots \ D^{\beta_m} u(t) \ -D^{\alpha_1} y_f^{IV}(t) \ \dots \ -D^{\alpha_n} y_f^{IV}(t) \right]^T \tag{27}$$

The IV vector should satisfy the following as

$$E\left[\varphi_f^{IV}(t) \varphi_f^T(t) \right] \text{ is non singular} \tag{28}$$

and

$$E\left[\varphi_f^{IV}(t) \varepsilon_f(t) \right] = 0 \tag{29}$$

where $E[\cdot]$ stands for the mathematical expectation. The continuous-time instrumental variable-based filter (CT IVSVF) estimation can be given as

$$\widehat{\theta}_{IVSVF} = \left(\mathbf{\Phi}_f^{IV^T} \mathbf{\Phi}_f \right)^{-1} \mathbf{\Phi}_f^{IV^T} \mathbf{Y}_f \tag{30}$$

where

$$\mathbf{\Phi}_f^{IV} = \left[\varphi_f^{IV}(T_s) \ \varphi_f^{IV}(2T_s) \ \dots \ \varphi_f^{IV}(NT_s) \right]^T \tag{31}$$

and the column vector $\mathbf{Y}_f$ is the same as (26). The implementation of CT IVSVF parameter estimation is summarized in the overall flow chart as shown in Fig. 3.

It should be noted that the simplified refined instrumental variable for continuous-time system identification (SRIVC) has been introduced to solve the problem of formulating unbiased parameter estimates. Although the SRIVC method is a powerful IV method for unbiased parameter estimation with proven statistical efficiency properties, the parameter estimation requires detailed modeling of the noise filter to obtain the statistical efficiency [43]. The prefilters and the highly colored noise present on the (filtered) Li-ion battery experimental measurements may require complex noise filters to achieve this statistical efficiency of SRIVC and require additional computations that can be avoided by choosing an instrument that is not optimal in terms of variance properties. Therefore, the above proposed IVSVF identification approach is selected to estimate parameters and compare performance/accuracy with LSSVF estimation method throughout this paper, knowing that the measurement noise will not be white in Li-ion battery system experimental data.

4. Continuous-time fractional differential model for a lithium ion battery

ECMs have been widely applied in BMS and compared with twelve commonly used ECMs, the first-order RC model (1-RC) is considered to be the best choice for Li-ion battery in terms of model complexity, model accuracy, and generalizability to multiple cells [44]. However, simple elements, such as capacitances, resistances, inductances or convective diffusion impedance, are not able to describe the experimental frequency dispersion result of a solid electrode/electrolyte interface [45]. A constant-phase element (CPE) can be generally applied to describe the capacitance dispersion of the frequency dispersion that is normally ascribed to distributed surface reactivity, electrode porosity, surface inhomogeneity, roughness or fractal geometry, current and potential distributions associated with electrode geometry instead of an ideal capacitor. Therefore, CPEs are used extensively in ECMs and the derived FDM structure is shown in Fig. 4. From the description in Fig. 4, it is worth mentioning that an ohmic resistor (R_0) can be applied to depict resistive impedance, a parallel circuit composed of a resistor (R_1) and a CPE, is used to represent the diffusion dynamic behavior.

The CPE is an equivalent electrical circuit component that appears currently in modeling the behavior of the imperfect dielectrics (partially capacitive and resistive) [46]. The electrical impedance can be expressed in terms of capacitance-like parameter C_1 and the differentiation order α ($\alpha \in \mathbb{R}^+$, $0 < \alpha < 1$)

$$Z_{CPE}(s) = \frac{1}{Y_{CPE}(s)} = \frac{1}{C_1 S^\alpha} \tag{32}$$

where the CPE admittance $Y_{CPE}(s)$, C_1 and α are frequency independent. Since constant phase is always $-90°$, the CPE as a circuit parameter is exhibiting limited behavior: an ideal capacitor for $\alpha = 1$, and a pure resistor for $\alpha = 0$ [47]. In this case (32), although CPE can be used as an extremely flexible fitting parameter to fit EIS data, it is not able to describe the meaning in terms of time constant distribution. The CT transfer function of the first-order FDM depicted in Fig. 4 can be derived as

$$H(s) = \frac{V_{OCV}(s) - V_0(s)}{I(s)} = \frac{V(s)}{I(s)} = R_0 + \frac{R_1}{1 + R_1 C_1 s^\alpha} \tag{33}$$

where $V_{OCV}(s) = \mathscr{L}\{v_{OCV}(t)\}$, $V_0(s) = \mathscr{L}\{v_0(t)\}$, $I(s) = \mathscr{L}\{i(t)\}$, and $\mathscr{L}\{\cdot\}$ is the notation for the Laplace transform.

The following relationship can be obtained from the whole circuit shown in Fig. 4

$$v_0 = v_{OCV} - v_1 - iR_0 \tag{34}$$

where i, v_0 and R_0 are the current, output voltage, and ohmic resistance, v_{OCV} is the open circuit voltage (OCV), v_1 and $\tau = R_1 C_1$ are the voltage and time constant of an RC circuit, respectively. The output function (34) consisted of state variable v_1, v_{OCV}, and implicit determining factor input current i.

All coefficients are replaced by the unknown circuit parameters, then the transfer function of first-order FDM (33) can be rewritten as

$$H(s) = \frac{V(s)}{I(s)} = \frac{b_0 + b_1 s^\alpha}{1 + a_1 s^\alpha} \tag{35}$$
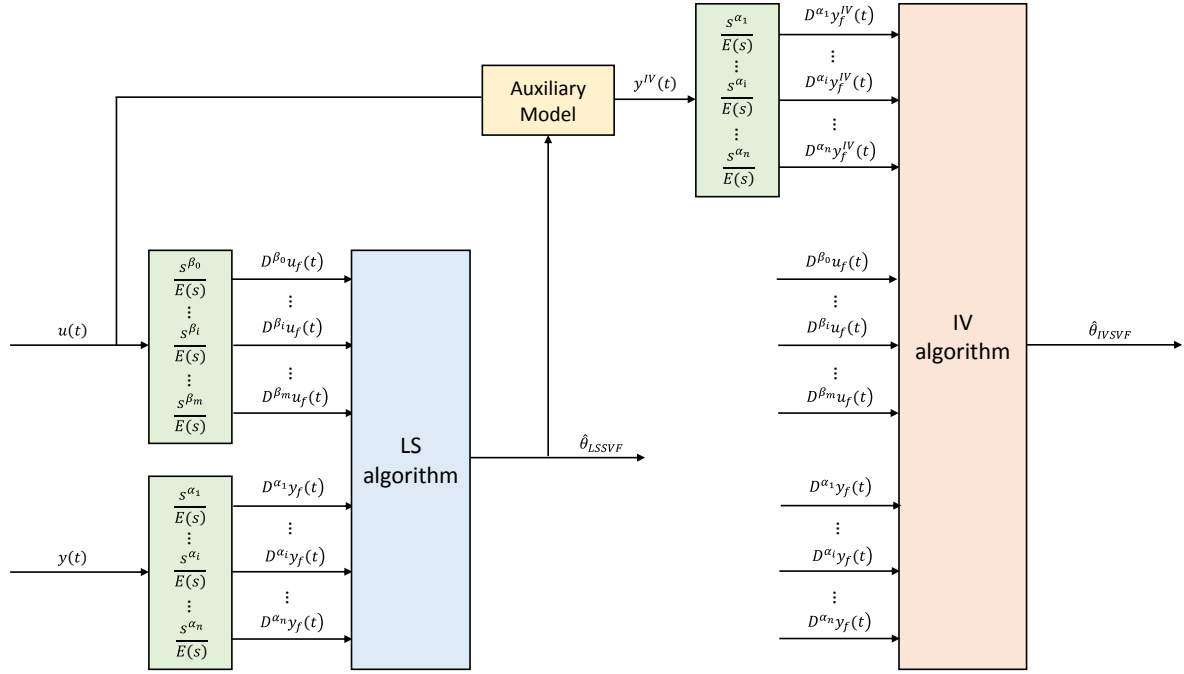
where the identified parameters are

Fig. 3. Implementation flow of continuous-time instrumental variable-based state-variable filter (CT IVSVF) parameter estimator.
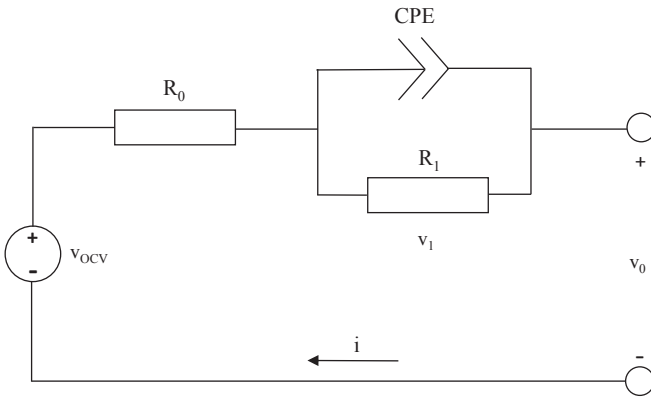

Fig. 4. Structure of the fractional differential model for Li-ion batteries.

$$b_0 = R_0 + R_1 \tag{36}$$

$$b_1 = R_0 R_1 C_1 \tag{37}$$

$$a_1 = R_1 C_1 \tag{38}$$

The above transfer function (35) can be described in a fractional differential equation form as

$$(1 + a_1 s^\alpha)V(s) = (b_0 + b_1 s^\alpha)I(s) \tag{39}$$

The current input $i(t)$ and voltage output $v(t) = v_{OCV}(t) - v_0(t)$ related with (39) can then be expressed as the following regression form

$$v(t) = \varphi_{FDM}(t)^T \theta_{FDM} \tag{40}$$

where the revised regression vector $\varphi_{FDM}(t)$ is defined as

$$\varphi_{FDM}(t) = [\, i(t) \ \ D^\alpha i(t) \ \ - D^\alpha v(t) \,]^T \tag{41}$$

and the parameters are denoted by the vector

$$\theta_{FDM} = [\, b_0 \ \ b_1 \ \ a_1 \,]^T \tag{42}$$

In most practical situations, the measured terminal battery voltage is usually the noise-free case, and it is actually corrupted by additive noises. Therefore, the complete equation for the battery system, with an equation error $\varepsilon(t)$, can be written in the regression form

$$v(t) = \varphi_{FDM}(t)^T \theta_{FDM} + \varepsilon(t) \tag{43}$$

Low-pass first-order SVF $L(s) = \frac{\gamma}{s+\gamma}$, as the most simple form in (19), is then applied to smoothen (filter) the time-derivative of current input and voltage output. Then, the filtered equation error can be defined as to estimate parameters

$$\varepsilon_f^*(t) = v_f(t) - \varphi_{FDM}^*(t)^T \theta_{FDM} \tag{44}$$

where the filtered regression vector can be given by

$$\varphi_{FDM}^*(t) = \left[\, i_f(t) \ \ D^\alpha i_f(t) \ \ - D^\alpha v_f(t) \,\right]^T \tag{45}$$

Subsequently, in order to validate the accuracy of the estimation, the fitness function $f(t)$ can be defined as follows

Table 1
Specific information of the Li-ion polymer battery under test.

Characterization	Lithium-ion polymer
Charge/discharge capacity	40.83/40.61 Ah
Nominal voltage	3.7 V
Minimum discharge voltage	2.7 V
Maximum charge voltage	4.2 V

(a) Battery characterization procedure.

(b) OCV of the battery under test.

(c) HPPC test profile.

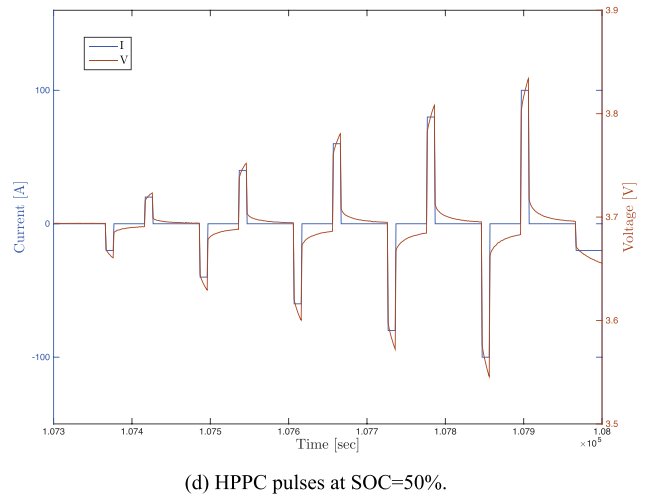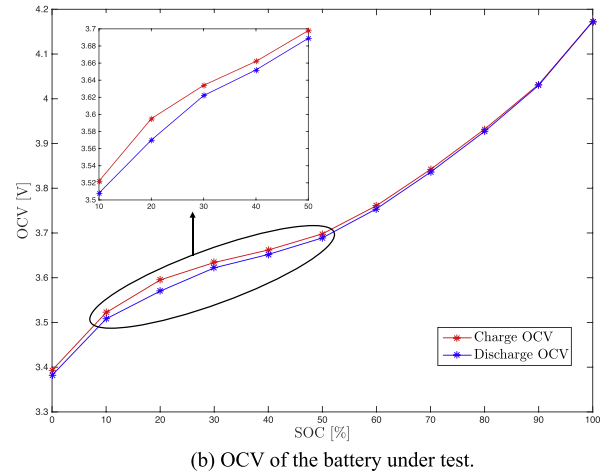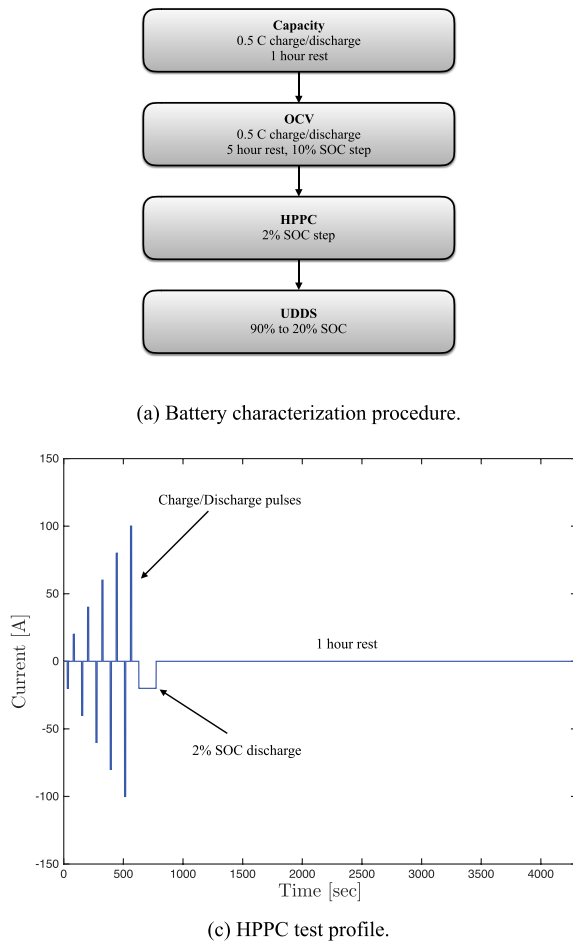(d) HPPC pulses at SOC=50%.

Fig. 5. Battery characterization and validation experiments.

$$f(t) = \left\| v_0(t) - v_{sim}(t) \right\|_2^2 \qquad (46)$$

where $v_0(t)$ is the tested battery terminal voltage and $v_{sim}(t)$ is the simulated battery voltage.

5. Model parameter identification and experimental results

The battery characterization experiments are conducted in order to estimate parameters and validate our proposed model of a Li-ion polymer battery cell.

5.1. Battery tests

Experiment characterization data of Li-ion polymer battery is continuously measured at room temperature (22–25° C) in the testing workbench. The specific information of the Li-ion polymer battery under test is shown in Table 1. As shown in Fig. 5a, a static capacity test, an OCV (open circuit voltage) test, a HPPC (Hybrid Pulse Power Characterization) test, and a UDDS (Urban Dynamometer Driving Schedule) test are consecutively conducted in the characterization tests. It should be noted that the sampling rate is 1 Hz in all characterization experiments.

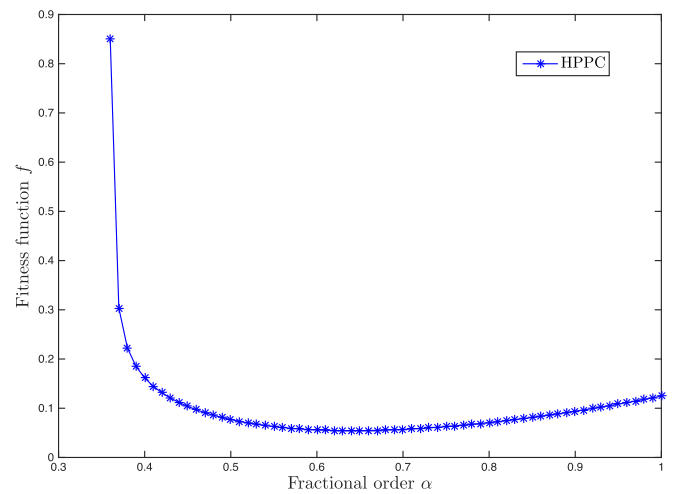There are three charge/discharge cycles in the static capacity

Fig. 6. Relationships between model accuracy and fractional order.

test. The Li-ion polymer battery is charged at 0.5C (constant current) in each cycle, until the battery terminal voltage can reach the maximum charge voltage (4.2 V). After that, the battery terminal voltage is maintained at the maximum value 4.2 V before the
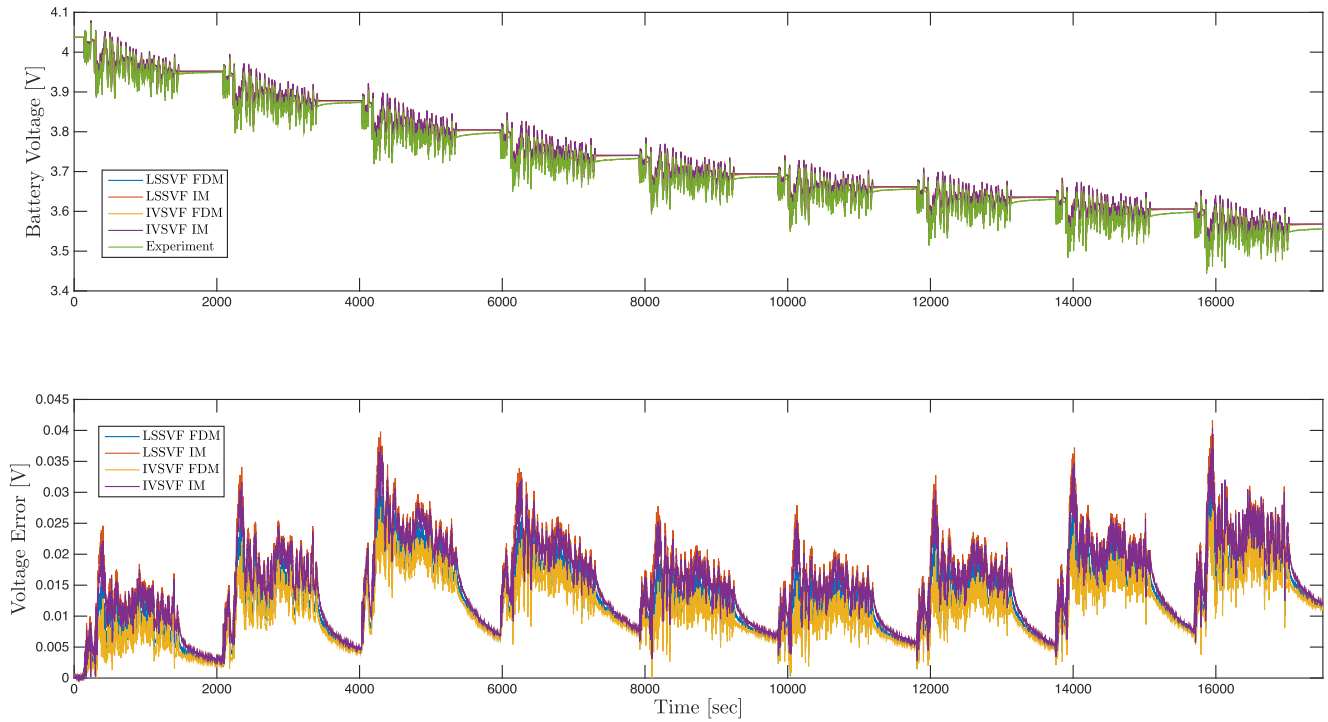
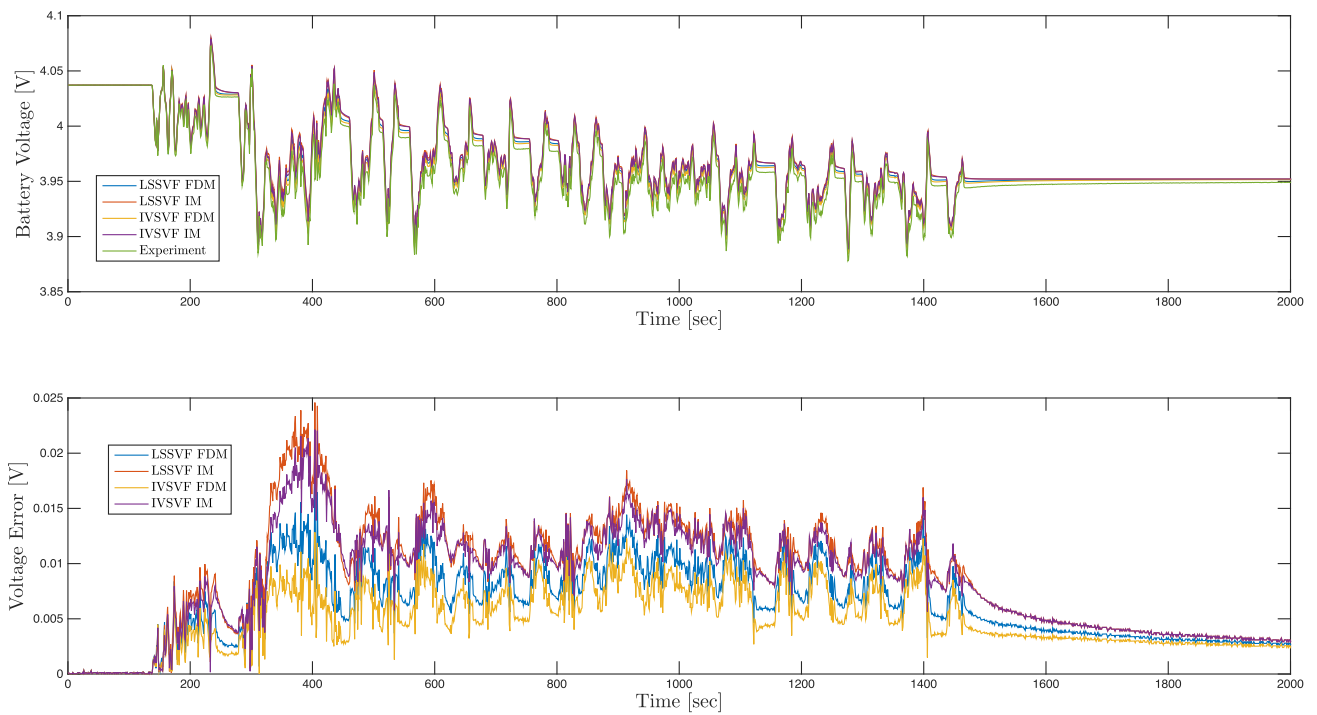**Fig. 7.** Voltage values and errors across all UDDS tests.

Fig. 8. Detailed voltage values and error between 0 s and 2000 s.

charge rate is below 1/20C. Then, the battery is discharged at a constant rate 0.5C before the battery terminal voltage reaches the minimum discharge voltage (2.7 V). Moreover, 1 h rest (0C) is then set after each charge/discharge cycle. The average value of all three charge/discharge cycles can be used to calculate the charge/discharge capacity.

As shown in Fig. 5b, the charge/discharge OCV-SOC experimental curves are measured at 10% SOC step with 0.5C charge/

discharge rate, and there is a 5 h rest between two neighboring charge/discharge cycles. As can be seen in Fig. 5b, the discharge OCV curve is slight lower than the charge curve at certain SOC range due to rate-dependent hysteresis. When SOC = 20%, the deviation between charge and discharge OCV curves reaches the maximum value 22.6 mV, as shown in small figure in Fig. 5b. It is worth noting that for the purpose of simplicity in calculation, the average value of the measured charge/discharge OCV-SOC curves is applied in the model identification.

Then, a HPPC test profile designed to measure dynamic power capability during both discharge and charge pulses is used in model parameter estimation. The HPPC test begins at 100% fully charged Li-ion battery and terminates after completing the final profile at 0% SOC with 2% SOC discharge step and 1 h rest between two consecutive charge/discharge cycles to allow the cell to return to a charge equilibrium condition before applying the next profile. The actual current input of one specific charge/discharge cycle of HPPC profile is shown in Fig. 5c. The HPPC current characterization profile and voltage response at SOC = 50% is recorded to establish the cells OCV behavior, which are enlarged in Fig. 5d.

UDDS datasets that can be used to be able to imitate the battery load of a car to represent city driving conditions at the specific temperatures, and voltage response records are used as model validation datasets in order to assess the simulated models. More procedure details can be found in our previous work [31].

5.2. Pre-determination of non-integer order

The fitness function $f(t)$ that describes the deviation between the simulated model output and experimental battery terminal voltage, is used to measure the model accuracy and validate the model performance. 1 Hz cut-off frequency for a low-pass filter is selected in order to pre-filter the input/output signals. As a matter of fact, the non-integer order α affects the model accuracy/performance. For this research, the fractional order α is selected from 0.01 to 1.0 with the step length 0.01. The identification process is performed at each α value, and the results are shown in Fig. 6. As can be seen from Fig. 6, the fitness function value typically changes when the value of the fractional order varies. It should be mentioned here that when the fractional orders are chosen from 0.01 to 0.35, the values of the fitness function are beyond the range compared with other selected fractional orders. Hence, the range of fractional order shown in Fig. 6 is chosen from 0.36 to 1 with step size 0.01. The model when the fractional order $\alpha = 0.64$ obtains the smallest value and obtains the best model accuracy/performance under HPPC test cycles. Thus, the optimized fractional order $\alpha = 0.64$ is chosen in the FDM to validate performance throughout this paper.

5.3. Validation results

In order to validate the model accuracy/performance of the aforementioned FDM, the optimized FDM (when $\alpha = 0.64$) is used to compare with same structure first-order integer model (IM) in (35) (when $\alpha = 1$) in both CT LSSVF and CT IVSVF system identification. The 1 Hz cut-off frequency is also selected as pre-filter SVF through the validation process. The validation result for UDDS test is shown in Fig. 7. The simulated and experimental battery voltage outputs, and voltage errors between the simulated models and experiment data are plotted in Fig. 7. And the zoom-in range results between 0 s and 2000 s are shown in Fig. 8. The results show that (1) the IM estimated by LSSVF method has the largest overall error compared with other estimated models; (2) the FDMs offers substantially better performance then IMs in both LSSVF and IVSVF methods; (3) the IVSVF identification method has better performance over LSSVF method in both FDM and IM, because the recent

Table 2
RMSE, MAE and MAD of model voltage estimation in whole UDDS validation.

	LSSVF IM	LSSVF FDM	IVSVF IM	IVSVF FDM
RMSE [mV]	16.87	12.88	16.30	9.15
MAE [mV]	15.39	11.70	14.92	8.20
MAD [mV]	0.57	0.48	0.49	0.37

presented IV method is less correlated (more independent) to the equation error; (4) FDM applied by IVSVF identification method appears the best performance compared with other estimated models under UDDS profile, which mainly consists of high frequency contents and is closer to the actual working conditions.

The root-mean-square error (RMSE), mean absolute error (MAE) and median absolute deviation (MAD) of above mentioned estimators over the full experimental period are chosen to list in Table 2. It validates that the proposed FDMs exhibit better overall performance and the explicitly RMSE, MAE and MAD of the FDM applied IVSVF system identification method is substantially smaller than other estimated models. It can be concluded from the above analysis that the proposed FDM applied IVSVF method characterizes the Li-ion battery more accurately and shows better performance than other models.

6. Conclusion

In this paper, a fractional differential model (FDM) and a parameter estimation strategy is proposed to approximate the nonlinear dynamic behavior of a Li-ion battery over a large operating range. The FDM is structured with a parallel circuit consisting of a constant phase element (CPE) and an ohmic resistor to resemble circuit-based Li-ion battery models. The parameter estimation strategy is formulated in continuous-time (CT) to allow direct estimation of parameters related to the fractional derivatives used in the model.

Compared with standard discrete-time (DT) methods, the proposed CT identification method is able to consistently estimate the parameters of the FDM and reproduce battery output response over a wide operating range. This is achieved by fixing the value of fractional differential order, and then use a state variable filter (SVF) to pre-filter and smoothen the time-derivatives of current and voltage signals. Parameter estimates are then obtained via both a standard least squares (LS) minimization and an iterative instrumental variable (IV) method to improve robustness against colored noise on the measured current and voltage signals.

The proposed FDM is a combination of the EIS experimental data and the 1-RC ECM model that has the similar structure with the commonly used RC model. Battery characterization experiments under different conditions are conducted in order to verify the accuracy and the performance of the proposed model. The comparison results indicate that CT IV identification methods show that smaller root-mean-square error (RMSE), mean absolute error (MAE), and median absolute deviation (MAD) compared to a standard CT LS optimization method.

Via experimental verification it is shown that the proposed FMD, where parameters are estimated via CT IV identification methods, can accurately capture the voltage and current signals over broad operation range of the Li-ion battery. The FDM is shown to provide better accuracy and prediction of battery terminal signals than the conventional linear differential equation models with integer derivatives. It is anticipated that the optimized FDM via CT IV parameter estimation method can be easily adapted in a battery management system to estimate and predict the battery dynamics for state of charge (SOC) and state of health (SOH) monitoring.

References

[1] Armand M, Tarascon J-M. Building better batteries. Nature 2008;451:652–7.
[2] Kanchev H, Lu D, Colas F, Lazarov V, Francois B. Energy management and operational planning of a microgrid with a PV-based active generator for smart grid applications. IEEE Trans Industrial Electron 2011;58:4583–92.
[3] Deng Z, Yang L, Cai Y, Deng H, Sun L. Online available capacity prediction and state of charge estimation based on advanced data-driven algorithms for lithium iron phosphate battery. Energy 2016;112:469–80.
[4] Felgenhauer MF, Pellow MA, Benson SM, Hamacher T. Evaluating co-benefits of battery and fuel cell vehicles in a community in California. Energy 2016;114:360–8.
[5] Xing Y, Ma EWM, Tsui KL, Pecht M. Battery management systems in electric and hybrid vehicles. Energies 2011;4:1840–57.
[6] Xia B, Mi C. A fault-tolerant voltage measurement method for series connected battery packs. J Power Sources 2016;308:83–96.
[7] Elsayed AT, Lashway CR, Mohammed OA. Advanced battery management and diagnostic system for smart grid infrastructure. IEEE Trans Smart Grid 2016;7:897–905.
[8] Li Y, Wang C, Gong J. A combination kalman filter approach for state of charge estimation of Lithium-ion battery considering model uncertainty. Energy 2016;109:933–46.
[9] Zhao X, de Callafon RA. Modeling of battery dynamics and hysteresis for power delivery prediction and SOC estimation. Appl Energy 2016;180:823–33.
[10] Santhanagopalan S, Guo Q, Ramadass P, White RE. Review of models for predicting the cycling performance of Lithium-ion batteries. J Power Sources 2006;156:620–8.
[11] Mastali M, Samadani E, Farhad S, Fraser R, Fowler M. Three-dimensional multi-particle electrochemical model of LiFePO4 cells based on a resistor network methodology. Electrochimica Acta 2016;190:574–87.
[12] Zhang D, Popov BN, White RE. Modeling lithium intercalation of a single spinel particle under potentiodynamic control. J Electrochem Soc 2000;147:831–8.
[13] Xiong R, Sun F, Chen Z, He H. A data-driven multi-scale extended Kalman filtering based parameter and state estimation approach of Lithium-ion polymer battery in electric vehicles. Appl Energy 2014;113:463–76.
[14] He H, Xiong R, Fan J. Evaluation of Lithium-ion battery equivalent circuit models for state of charge estimation by an experimental approach. Energies 2011;4:582–98.
[15] Jossen A. Fundamentals of battery dynamics. J Power Sources 2006;154:530–8.
[16] Xu J, Mi CC, Cao B, Cao J. A new method to estimate the state of charge of Lithium-ion batteries based on the battery impedance model. J Power Sources 2013;233:277–84.
[17] M. Eckert, L. Klsch, S. Hohmann, Fractional algebraic identification of the distribution of relaxation times of battery cells, in: 2015 54th IEEE Conference on Decision and Control (CDC), pp. 2101–2108.
[18] Hu Y, Yurkovich S. Linear parameter varying battery model identification using subspace methods. J Power Sources 2011;196:2913–23.
[19] Lee S, Kim J, Lee J, Cho BH. State-of-charge and capacity estimation of Lithium-ion battery using a new open-circuit voltage versus state-of-charge. J Power Sources 2008;185:1367–73.
[20] Rao GP, Unbehauen H. Identification of continuous-time systems. IEE Proc - Control Theory Appl 2006;153:185–220.
[21] Young PC, Garnier H, Gilson M. Refined instrumental variable identification of continuous-time hybrid box-Jenkins models. In: Garnier H, Wang L, editors. Identification of continuous-time models from sampled data, advances in industrial control. Springer London; 2008. p. 91–131. http://dx.doi.org/10.1007/978-1-84800-161-9_4.
[22] Schorsch J, Garnier H, Gilson M, Young PC. Instrumental variable methods for identifying partial differential equation models. Int J Control 2013;86:2325–35.
[23] Laurain V, Gilson M, Tth R, Garnier H. Refined instrumental variable methods for identification of LPV BoxJenkins models. Automatica 2010;46:959–67.
[24] Oustaloup A, Levron F, Mathieu B, Nanot FM. Frequency-band complex non-integer differentiator: characterization and synthesis. IEEE Trans Circuits Syst I Fundam Theory Appl 2000;47:25–39.
[25] Petr I. Fractional-order nonlinear systems, nonlinear physical science. Berlin, Heidelberg: Springer Berlin Heidelberg; 2011.
[26] Monje CA, Chen Y, Vinagre BM, Xue D, Feliu V. Fractional-order systems and controls, advances in industrial control. London: Springer London; 2010.
[27] Jiang Y, Zhao X, Valibeygi A, de Callafon RA. Dynamic prediction of power storage and delivery by data-based fractional differential models of a lithium iron phosphate battery. Energies 2016;9:590.
[28] Kaczorek T, Rogowski K. Fractional linear systems and electrical circuits, volume 13 of studies in systems, decision and control. Cham: Springer International Publishing; 2015.
[29] Kexue L, Jigen P. Laplace transform and fractional differential equations. Appl Math Lett 2011;24:2019–23.
[30] A. Tepljakov, E. Petlenkov, J. Belikov, FOMCON: fractional-order modeling and control toolbox for MATLAB, in: mixed design of integrated circuits and systems (MIXDES), 2011 Proceedings of the 18th international conference, pp. 684–689.
[31] Xia B, Zhao X, de Callafon R, Garnier H, Nguyen T, Mi C. Accurate Lithium-ion battery parameter estimation with continuous-time system identification methods. Appl Energy 2016;179:426–36.
[32] Garnier H, Mensler M, Richard A. Continuous-time model identification from sampled data: implementation issues and performance evaluation. Int J Control 2003;76:1337–57.
[33] Remmlinger J, Buchholz M, Meiler M, Bernreuter P, Dietmayer K. State-of-health monitoring of Lithium-ion batteries in electric vehicles by on-board internal resistance estimation. J Power Sources 2011;196:5357–63.
[34] Garnier H, Young PC. The advantages of directly identifying continuous-time transfer function models in practical applications. Int J Control 2014;87:1319–38.
[35] Wu H, Yuan S, Zhang X, Yin C, Ma X. Model parameter estimation approach based on incremental analysis for Lithium-ion batteries without using open circuit voltage. J Power Sources 2015;287:108–18.
[36] Yuan S, Wu H, Ma X, Yin C. Stability analysis for Li-ion battery model parameters and state of charge estimation by measurement uncertainty consideration. Energies 2015;8:7729–51.
[37] Garnier H. Direct continuous-time approaches to system identification. Overview and benefits for practical applications. Eur J Control 2015;24:50–62.
[38] Garnier H, Bitmead RR, de Callafon RA. Direct continuous-time model identification of high-powered light-emitting diodes from rapidly sampled thermal step response data. IFAC Proc Vol 2014;47:6430–5.
[39] Ljung L. System identification. In: Prochzka A, Uhl J, Rayner PWJ, Kingsbury NG, editors. Signal analysis and prediction, applied and numerical harmonic analysis. Birkhuser Boston; 1998. p. 163–73.
[40] Diethelm K. The analysis of fractional differential equations, volume 2004 of Lecture Notes in Mathematics. Berlin, Heidelberg: Springer Berlin Heidelberg; 2010.
[41] Garnier H, Gilson M, Bastogne T, Mensler M. The CONTSID Toolbox: a software support for data-based continuous-time modelling. In: Garnier H, Wang L, editors. Identification of continuous-time models from sampled data, advances in industrial control. Springer London; 2008. p. 249–90.
[42] R. Malti, S. Victor, A. Oustaloup, H. Garnier, An optimal instrumental variable method for continuous-time fractional model identification, in: 17th IFAC world congress, p. XX.
[43] Young P, Garnier H, Gilson M. AN optimal instrumental variable approach for identifying hybrid continuous-time box-Jenkins models. IFAC Proc Vol 2006;39:225–30.
[44] Hu X, Li S, Peng H. A comparative study of equivalent circuit models for Li-ion batteries. J Power Sources 2012;198:359–67.
[45] Jorcin J-B, Orazem ME, Pbre N, Tribollet B. CPE analysis by local electrochemical impedance spectroscopy. Electrochimica Acta 2006;51:1473–9.
[46] Alexander CL, Tribollet B, Orazem ME. Contribution of surface distributions to constant-phase-element (CPE) behavior: 1. Influence of roughness. Electrochimica Acta 2015;173:416–24.
[47] Zoltowski P. On the electrical capacitance of interfaces exhibiting constant phase element behaviour. J Electroanal Chem 1998;443:149–54.